Mater. Res. Soc. Symp. Proc. Vol. 1260 © 2010 Materials Research Society 1260-T10-03

Phase-separation in $Zn_xCd_{1-x}Se$/C Core/shell nanocrystals studied with cathodoluminescence spectroscopy

Yevgeni Estrin,[1] Daniel H. Rich,[1] Ofer Moshe,[1] Sayan Bhattacharyya,[2] and Aharon Gedanken[3]

[1]Department of Physics, The Ilse Katz Institute for Nanoscience and Nanotechnology, Ben-Gurion University of the Negev, P.O.Box 653, Beer-Sheva 84105, Israel
[2]Department of Chemical Sciences, Indian Institute of Science Education and Research, Kolkata, Mohanpur - 741252, Nadia, W.B., India
[3]Department of Chemistry and Kanbar Laboratory for Nanomaterials at the Bar-Ilan University Center for Advanced Materials and Nanotechnology, Bar-Ilan University, Ramat-Gan, Israel

ABSTRACT

$Zn_xCd_{1-x}Se$/C core/shell nanocrystals with 31-39 nm diameter semiconductor cores and 11-25 nm-thick carbon shells were synthesized from solid state precursors. Transmission electron microscopy showed striations on a scale of ~1 – 5 nm in the nanocrystals that are indicative of a composition modulation, and reveal a chemical phase separation and possible spinodal decomposition within the nanocrystals. Such a composition modulation within the ternary nanocrystals represents a rarely reported phenomenon that could lead to additional applications. The optical properties and carrier relaxation kinetics of the nanocrystals were examined with variable excitation cathodoluminescence (CL). As the excitation level is increased, carrier filling in two-dimensional (2D) phase-separated Cd-rich regions leads to a partial saturation of states before the onset of carrier filling in the higher bandgap homogenous $Zn_{0.47}Cd_{0.53}Se$ regions. In order to model the state filling using Fermi-Dirac statistics for non-interacting carriers, a random quantum well model was used to determine the electron and hole eigensates in the Cd-rich regions of the nanocrystals.

INTRODUCTION

Much effort has been expended recently in studying the synthesis of $Zn_xCd_{1-x}Se$ materials in the form of nanowires,[1] nanorods,[2] nanocrystals,[3] and quantum dots.[4] Applications in biological labeling, light sources, and photovoltaics are envisioned.[5,6] The chemical phase separation during the growth and synthesis of strained ternary semiconductors can yield additional quantum effects if the spatial modulation is less than ~10 nm, and possibly provide for additional device applications, such as, e.g., the spontaneous formation of quantum wires during the growth of $(InP)_2/(GaP)_2$ bilayer superlattices on GaAs.[7,8,9] Chemical phase separation within ternary II-VI crystals is a rare phenomenon, but has been predicted and observed.[10] Using high-resolution transmission electron microscopy (TEM), a spinodal-like phase separation was observed for $Cd_xZn_{1-x}Te$ layers grown on GaAs substrates.[11] Of particular relevance is a study of phase separation for $Zn_xCd_{1-x}Se$ epilayers grown on InP using organometallic vapor phase epitaxy which exhibited various mixed chemical phases having compositions, *x*, ranging from 0 to 1, as studied by cathodoluminescence (CL) and x-ray diffraction (XRD).[12]

In our recent study of $Zn_xCd_{1-x}Se$/C core-shell nanocrystals, TEM showed two-dimensional (2D) striations in the nanocrystals that are indicative of a composition modulation along a preferred crystallographic direction and reveal a chemical phase separation.[13] CL of these

nanocrystals further showed that a composition modulation, Δx, of ~0.11 is consistent with a broadened emission and set of decomposed peaks in spatially integrated CL spectra.[13,14] In this paper, we further build on the results of phase separation in $Zn_xCd_{1-x}Se$ nanocrystals by examining the excitation dependence of CL spectra that exhibit multiple components. Excitation-dependent effects in 2D Cd-rich regions of the nanocrystals are modeled with a random quantum well (RQW) approximation. Unexpected phenomena, such as phase separation in II-VI nanocrystals, may provide a means to create lower dimensional quantum nanostructures.

EXPERIMENT

$Zn_xCd_{1-x}Se$/C core/shell nanocrystals were synthesized using a simple technique of pyrolyzing the solid state precursors within a sealed reactor at higher temperatures and under autogenic pressures.[13] The CL experiments were performed on a modified JSM-5910 scanning electron microscope (SEM), and the CL detection system has been described previously in detail.[15] An *e*-beam energy (E_b) of 15 keV was used. A UV multialkali photomultiplier tube operating in the 185–850 nm spectral range enabled the photon counting of the luminescence that was dispersed by a 0.25 m monochromator. The spectral resolution was ~1 nm.

RESULTS AND DISCUSSION

The one-step synthesis method is useful in creating a carbon shell *in situ* without the use of surfactants or carbon containing feedstock gas, and hence is an environmentally friendly method. The carbon shell ensures excellent surface passivation of the nanocrystals, eliminates the cytotoxicity of the nanocrystal core for biological applications and permits adequate transparency for detecting optical activity. The nanocrystals had a 31-39 nm semiconducting core and 11-25 nm carbon shell. In two step reactions (samples ZC1 and ZC2), spherical nanostructures were mostly observed, whereas a mixture of spherical and tripod nanostructures were obtained in a one-step reaction (sample ZC3).[13] The resulting cubic and hexagonal structural phases and Zn compositions *x* were determined by Rietveld analysis of the XRD patterns and previously reported in detail.[13] The carbon encapsulation offers excellent protection to the nanocrystal core, is stable during the *e*-beam exposure in the CL measurements,[13] and is an added advantage for biological applications.

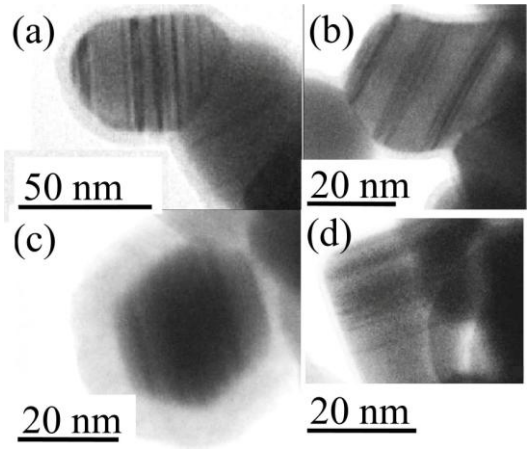

Figure 1. Bright-field TEM images of the nanocrystals for samples ZC1 (a), ZC2 (b), and ZC3, both (c) and (d).

Figure 1 shows bright field TEM images of single nanocrystals from the three samples. A hexagonal ~31 nm core is shielded by a ~8 nm carbon shell in Fig. 1(c). Significant striations are observed in the four TEM images. These striations indicate a composition modulation along a crystallographic direction normal to the stripes. Such a composition modulation could result from spinodal decomposition within the nanocrystals, with such fluctuations occurring on a ~1-5 nm size scale. Therefore, such a phase separation occurs within the quantum confinement regime for electrons and holes in the nanocrystal and leads to expected local modifications of the optical and electronic properties. In Fig. 2, we show

local CL spectra acquired at six different locations on sample ZC3 for T = 60 K. The local CL spectra were acquired by fixing the *e*-beam injection position during the measurements. For the case of CL spectra obtained by local excitation, we observed emission from groups of nanocrystals that usually exhibited one to three components, with the present case showing two and three components in Fig. 2. The CL spectra were decomposed into a sum of discrete Gaussian peaks, as indicated by the labels P_2-P_4 in Fig. 2. These labels correspond to similar CL peaks observed in an analysis of spatially integrated CL spectra for the same ZC3 sample.[13,14] The intensity of the longer wavelength P_2 component decreases relative to that of P_3 as the temperature increases from 60 to 90 K, suggesting that carrier excitation from the phase-separated region to the homogenous regions [$x \approx 0.47$ (*h*)] of the nanocrystal occurs over this temperature range.[14] Considerable spatial variations in the spectral lineshape were observed during local CL spectroscopy, and representative spectra showing two and three components are shown in Fig. 2.

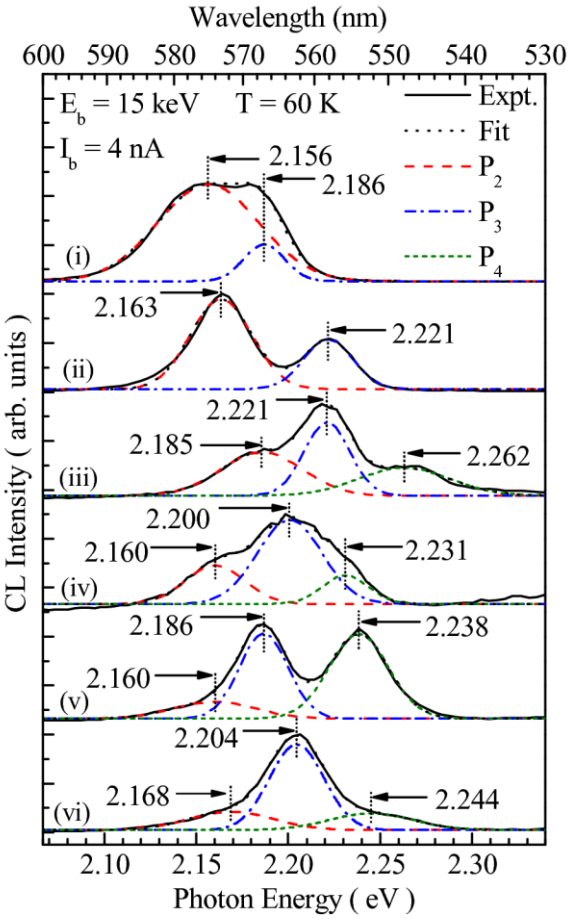

Figure 2. Local CL spectroscopy and decomposition into Gaussian components for six different locations on sample ZC3.

Previously, using XRD and the compositional dependence of the $Zn_xCd_{1-x}Se$ bandgap emission energy, we attributed peak P_3 (~2.196 eV) as due to a combination of emissions from nanocrystals possessing homogenous compositions, *x*, of ~0.47 (*h*) and ~0.50 (*c*), in which *h* and *c* refer to the hexagonal and cubic phases, respectively.[13]

Table I. Zn compositions for P_2-P_4

CL Spec.	x_2	x_3	x_4
(i)	0.418	0.449	---
(ii)	0.425	0.485	---
(iii)	0.448	0.484	0.525
(iv)	0.422	0.463	0.494
(v)	0.422	0.449	0.501
(vi)	0.431	0.467	0.507

Moreover, peaks P_2 (2.152 eV) and P_4 (2.255 eV) correlate with emissions from regions exhibiting phase separation into compositions of 0.41 (*h*) and 0.52 (*h*), respectively, as the analysis was based on spectrally integrated CL spectroscopy over a 128 × 96 μm^2 region.[13] The local CL spectra shown in Fig. 2 were however acquired by a fixed *e*-beam injection and so spatial variations in the P_2-P_4 peak energy positions are expected, owing to the random fluctuations in the ternary composition *x*.

In Table I, we assign compositions x_2-x_4 according to the peak energies of the decomposed Gaussian components P_2-P_4 for the CL spectra, as denoted from (i) to (vi) in Fig. 2. The following expression (in units of eV) for the Zn composition-dependent bandgap was used to determine the compositions (x_2-x_4) for the hexagonal phase corresponding to the peak energy positions of P_2-P_4:[13]

$$E^h_g(x) = 1.84 + 0.57\,x + 0.45\,x^2. \qquad (1)$$

Notwithstanding the variations in compositions associated with P_3 (i.e., regions exhibiting an homogenous alloy compositon x_3), compositions x_2 and x_4 are roughly symmetrically displaced about x_3, as expected for a ternary crystal that exhibits a chemical phase separation. Variations between individual and groups of nanocrystals will yield random fluctuations in the composition modulation of approximately $\pm |x_4 - x_2|/2$ about x_3 and in the composition x_3 itself, as observed in Fig. 2 and Table I. Several regions of the nanocrystals exhibited only the lowest energy components, P_2 and P_3, as observed in (i) and (ii) of Fig. 2. We hypothesize that the absence of P_4 emission in these regions relates to variations in the carrier collection and recombination dynamics which depend on unknown factors such as the specific geometrical structure and connectivity of the Zn-rich and homogenous regions and the local density of defects that will affect the radiative efficiency.

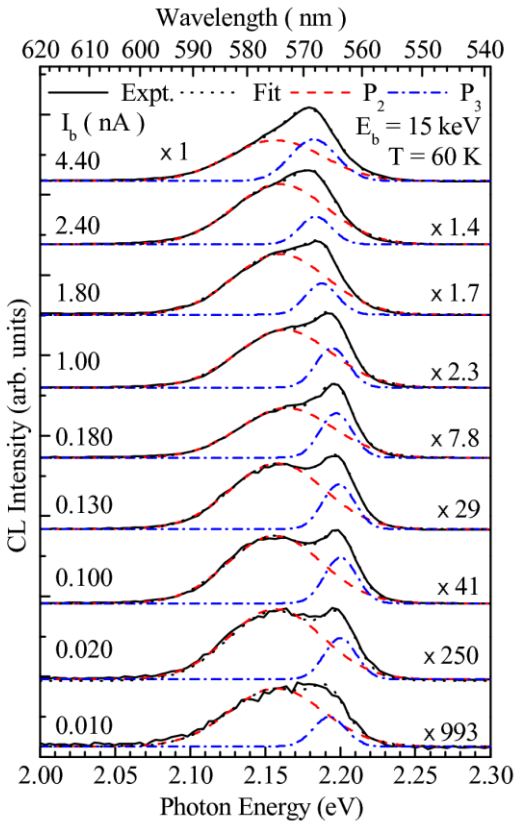

Figure 3. Variable excitation local CL spectroscopy of sample ZC3.

Figure 3 shows the excitation dependence for various I_b at T = 60 K in a similar but not identical group of nanocrystals of sample ZC3 that yielded the results for two component regions, P_2 and P_3, in Fig. 2. For the lowest beam current shown, I_b = 10 pA, a single broad luminescence peak rapidly evolves into the expected double-peaked lineshape observed in Fig. 2(a). Again, we have decomposed the local CL spectra into Gaussian components, P_2 and P_3, as shown. The onset of the increase in intensity of the higher-energy component (i.e., the P_3 component) for $I_b \geq 180$ pA reflects the rapid phase and real space filling of states in the Cd-rich regions, leading to an enhanced carrier transfer to the homogenous alloy. The average 2D carrier density, n_{ex}, in a $Zn_{0.47}Cd_{0.53}Se$ nanocrystal with a 35 nm-thick core and 10 Cd-rich 2D regions (as evidenced from the ~10 striations per nanocrystal in the TEM images of Fig. 1) is estimated as $n_{ex} \approx I_b \cdot 2.5 \times 10^{12}$ cm^{-2} per striation with the *e*-beam current in units of nA.[14] In Fig. 4, the intensity ratio I_{p3}/I_{p2} as a function of I_b is shown with black dots, revealing a gradual increase in I_{p3}/I_{p2} as phase space and real space filling of carriers occur in the two-dimensional (2D) Cd-rich regions.

We have quantitatively modeled the band filling in the 2D Cd-rich regions by employing a random quantum well (RQW) approximation. In this model, we assume a fixed composition modulation of Δx = 0.12, with three separate structures composed of 4, 5, and 7 QWs whose well width and barrier thickness varied from 3 – 6 nm, 2.6 – 4.6 nm, and 1.6 – 3.6 nm, respectively. The total width of the multi-QW (MQW) was constrained to be ~36 nm, with individual well and barrier widths varying stochastically within the above three ranges for the three MQW structures. The stochastic nature of the striated regions in the TEM images of Fig. 1 provides the motivation for such a RQW model and is indeed consistent with observed random variations in the peak positions P_2-P_4 that were observed in local CL spectra (Fig. 2). The energy states in the RQW were obtained using a standard transfer matrix method (TMM) for multiple coupled QWs in the

effective mass approximation for electrons and holes.[16] Electron and hole effective masses were taken as $(0.13 + 0.03x)\ m_e$ and $(0.45 + 0.15x)\ m_e$, respectively.[17,18] A conduction to valence band offset ratio of $\Delta E_c/\Delta E_v = 4$ for wurtzite $Zn_xCd_{1-x}Se$ is assumed,[19] along with the composition-dependent bandap of Eq. (1). For a given excess carrier concentration, n_{ex}, using the two-dimensional density of states which is proportional to the appropriate in-plane effective masses, we calculated the population of each quantized state and the quasi-Fermi levels for electrons and holes, ϕ_e and ϕ_h. The electron and heavy-hole carrier densities, n_i^e and n_j^h, in these quantized states can be determined by integrating the product of the 2D density of states and the Fermi-Dirac function. The quasi-Fermi levels, $\phi_{e,h}$, are therefore determined by solutions of the following equations:

$$n_i^e = \frac{4\pi m_e}{h^2}\left\{k_B T \ln\left[1+\exp\left(\frac{E_i^e-\varphi_e}{kT}\right)\right]-E_i^e+\varphi_e\right\}\ ;$$

$$n_j^h = \frac{4\pi m_h}{h^2}\left\{k_B T \ln\left[1+\exp\left(\frac{\varphi_h-E_j^h}{kT}\right)\right]-\varphi_h+E_j^h\right\}\ ;$$

$$n_{ex} = \sum_{i=1}^{S_e} n_i^e = \sum_{j=1}^{S_h} n_j^h\ , \qquad (2)$$

where S_e and S_h represent the number of energy states used in the calculations for electrons and heavy holes, respectively. In this calculation, we have used $S_e = S_h = N_W$, where N_W is the number of QWs in the structure. Due to the variable number of excited states that depend on the well widths in the RQW, we have constrained $S_e = S_h$, so as to represent carrier filling of only the N_W lowest electron and hole states for simplicity.

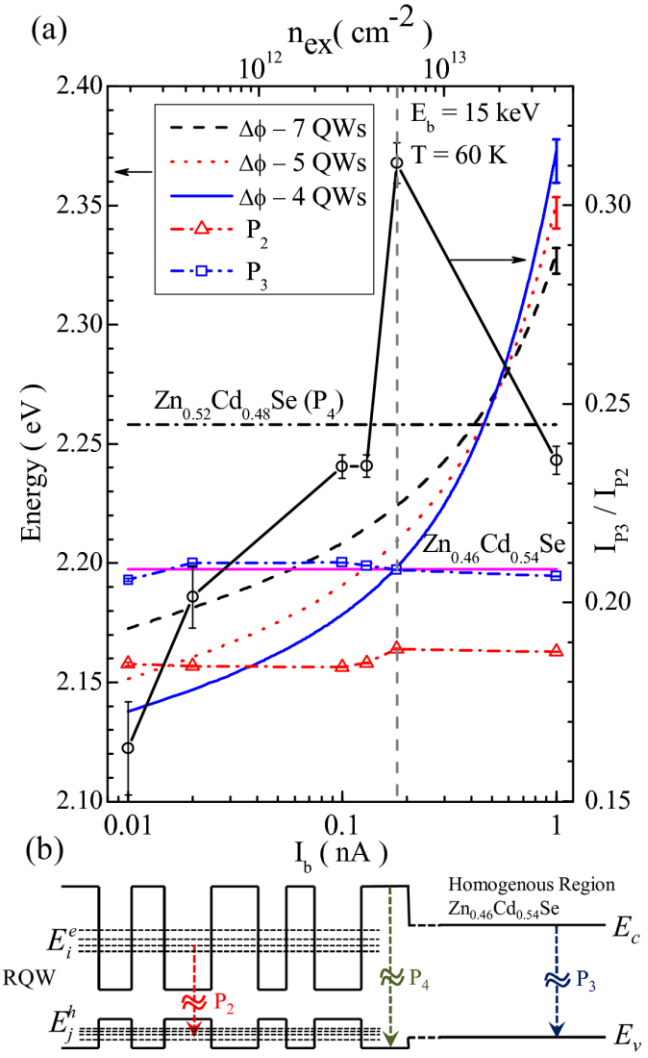

Figure 4. Quasi-Fermi level difference, $\Delta\phi = \phi_e - \phi_h$, and I_{p3}/I_{p2} as a function of *e*-beam current, I_b, and excitation density, n_{ex} in (a) and schematic band-diagram in (b).

The results of the band filling in the RQW model are shown in Fig. 4. The difference in quasi-Fermi levels, $\Delta\phi = \phi_e - \phi_h$, versus I_b and n_{ex} is shown for the three cases of 4, 5, and 7 QWs, which comprise the MQW. TMM calculations using the RQW approximation were carried out 20 times for each of the three cases, and resulted in 20 sets of MQW structures and 20 sets of corresponding eigenstates. For each of the 20 sets, we then calculated $\Delta\phi$ and its average, which is shown in Fig. 4 for the three cases of 4, 5, and 7 QWs. Standard deviations, $\sigma_{\Delta\phi}$, of $\Delta\phi$ for each case are indicated with the corresponding error bar at the top of each of the $\Delta\phi$ curves. Thus, $\sigma_{\Delta\phi}$ represents the statistical fluctuation of the quasi-Fermi level differences that can be expected in the RQW model. Also, in Fig. 4, we show the positions of the peaks P_2 (triangles) and P_3

(squares) that were obtained from the Gaussian components shown in Fig. 3. A rapid increase in the intensity ratio I_{p3}/I_{p2} is observed for I_b = 0.18 nA. This also correlates with a ~10 meV shift in the P_2 component and a crossing of $\Delta\phi$ for the case of 4-QWs at the position of the P_3 peak. We observe that for the case of 4 QWs and I_b = 0.18 nA, a sudden increase in carrier transfer occurs when $\Delta\phi \approx E_{P3}$, the P_3 energy position, which is the position of the homogenous alloy region of $x \approx 0.46$. Thus, we conclude that for this particular group of nanocrystals, the RQW with 4 QWs yields a result consistent with carrier filling and an enhanced carrier transfer to the homogenous alloy with its concomitant increase in intensity (i.e., an increase in I_{p3}/I_{p2}) when the excitation density reaches the experimental value determined by an *e*-beam current of 0.18 nA .

In conclusion, the optical properties and the excitation-dependent carrier filling of $Zn_xCd_{1-x}Se$/C core/shell nanocrystals with a compositional phase separation were examined with CL. The CL spectral lineshape varied with location and was found to depend on the level of excitation. As the excitation level is increased, carrier filling in two-dimensional (2D) phase-separated Cd-rich regions leads to a partial saturation of states before the onset of carrier filling in the higher bandgap homogenous $Zn_{0.47}Cd_{0.53}Se$ regions. In order to model the state filling using Fermi-Dirac statistics for free carriers, a random quantum well (RQW) model was used to determine the electron and hole eigensates in the Cd-rich regions of the nanocrystals. These results illustrate that compositional phase separation on the scale of ~1-5 nm in II-VI nanocrystals can lead to potentially useful quantum effects and interesting optical properties.

REFERENCES

1. X. T. Zhang, Z. Liu, Q. Li, S. K. Hark, J. Phys. Chem. B **109**, 17913 (2005).
2. H. Lee et. al., J. Chem. Phys. **125**, 164711 (2006).
3. Y.-M. Sung, Y.-J. Lee, and K.-S. Park, J. Am. Chem. Soc. **128**, 9002 (2006).
4. B. P. Zhang, Y. Q. Li, T. Yasuda, W. X. Wang, Y. Segawa, K. Edamatsu and T. Itoh, Appl. Phys. Lett. **73**, 1266 (1998).
5. J. I. Kim and J.-K. Lee, Adv. Funct. Mater. **16**, 2077 (2006).
6. Y. Zheng, Z. Yang and J. Y. Ying, Adv. Mater. **19**, 1475 (2007).
7. K. C. Hsieh, J. N. Baillargeon, and K. Y. Cheng, Appl. Phys. Lett. **57**,2244 (1990).
8. A. Mascarenhas, R. G. Alonso, G. S. Horner, S. Froyen, K. C. Hsieh, and K. Y. Cheng, Phys. Rev. B **48**, 4907 (1993).
9. Y. Tang, D. H. Rich, A. M. Moy and K. Y. Cheng, J. Vac. Sci. Technol. B **15**, 1034 (1997).
10. A. Marbeuf , R. Druilhe, R. Triboulet, G. Patriarche, J. Cryst. Growth **117**, 10 (1992).
11. H. S. Lee et. al., J. Appl. Phys. **99**, 093512 (2006).
12. X. B. Zhang and S. K. Hark, J. Cryst. Growth **223**, 512 (2001).
13. S. Bhattacharyya, Y. Estrin, O. Moshe, D. H. Rich, L. A. Solovyov, and A. Gedanken, ACS Nano **3**, 1864 (2009).
14. Y. Estrin, D. H. Rich, O. Moshe, S. Bhattacharyya and A. Gedanken**,** Appl. Phys. Lett. **95**, 181903 (2009).
15. H. T. Lin, D. H. Rich, A. Konkar, P. Chen, and A. Madhukar, J. Appl. Phys. **81**, 3186 (1997).
16. R. M. Kolbas and N. Holonyak, Am. J. Phys. 52, 431 (1984).
17. J. Müller et. al., Nano Lett. **5**, 2044 (2005).
18. C. Targer-Cowan et. al., Semicond. Sci. Technol. **7**, 536 (1992).
19. M. V. Maksimov, I. L. Krestnikov, S. V. Ivanov, N. N. Ledentsov, and S. V. Sorokin, Semiconductors **31**, 800 (1997).